JGR Solid Earth

RESEARCH ARTICLE
10.1029/2024JB029936

Bayesian Preprocessing for Palaeomagnetic Sediment Records Using a Flexible Lock-In Function Approach

L. Bohsung[1,2], **M. Schanner**[1,2], **M. Korte**[1], **and M. Holschneider**[2]

[1]GFZ German Research Centre for Geosciences, Potsdam, Germany, [2]Applied Mathematics, University of Potsdam, Potsdam, Germany

Key Points:

- We present *sedprep*, a Python package that can be used to preprocess palaeomagnetic sediment records
- *sedprep* estimates declination offsets, RPI calibration, inclination shallowing factor, and lock-in function parameters simultaneously
- The final step applies the estimated parameters to provide the calibrated and corrected palaeomagnetic signal

Supporting Information:

Supporting Information may be found in the online version of this article.

Correspondence to:

L. Bohsung,
lbohsung@gfz-potsdam.de

Citation:

Bohsung, L., Schanner, M., Korte, M., & Holschneider, M. (2024). Bayesian preprocessing for palaeomagnetic sediment records using a flexible lock-in Function approach. *Journal of Geophysical Research: Solid Earth*, *129*, e2024JB029936. https://doi.org/10.1029/2024JB029936

Received 15 JUL 2024
Accepted 16 DEC 2024

Author Contributions:

Conceptualization: L. Bohsung, M. Schanner, M. Korte, M. Holschneider
Data curation: L. Bohsung, M. Schanner
Formal analysis: L. Bohsung, M. Schanner
Funding acquisition: M. Schanner, M. Korte, M. Holschneider
Investigation: L. Bohsung, M. Schanner, M. Korte, M. Holschneider
Methodology: L. Bohsung, M. Schanner, M. Korte, M. Holschneider
Project administration: M. Korte, M. Holschneider
Resources: L. Bohsung, M. Schanner
Software: L. Bohsung, M. Schanner
Supervision: M. Korte, M. Holschneider
Validation: L. Bohsung, M. Schanner, M. Korte, M. Holschneider

Abstract Geomagnetic field models covering past millennia rely on two main data sources: archaeomagnetic data, that provide snapshots of the geomagnetic field at specific locations, and sediment records, that deliver time series of the geomagnetic field from individual cores. The limited temporal and spatial global coverage with archaeomagnetic data necessitates use of sediment data, especially when models go further back in time. However, the accurate preprocessing and interpretation of sediment data is crucial. Unlike archaeomagnetic data, sediment data does not provide absolute values for intensities and declinations; instead, it represents relative variations. The detrital remanent magnetization (DRM) of sediment records is influenced by various depositional (dDRM) effects that can result in inclination shallowing, as well as post-depositional (pDRM) processes that cause a delayed and smoothed signal. To address the distortion associated with the pDRM effects, a novel class of flexible parameterized lock-in functions has been proposed. These lock-in functions involve four parameters, which are estimated using a Bayesian modeling technique and archaeomagnetic data. By extending the space of hyperparameters to include the calibration factor for intensities, the declination offsets and the inclination shallowing factor, we present a fully Bayesian preprocessing method for sediment records in form of a Python package, called *sedprep*. By applying the estimated parameters to the raw sediment data *sedprep* is able to provide a calibrated and preprocessed palaeomagnetic record.

Plain Language Summary Our research introduces a new Python package called *sedprep* that helps scientists better understand ancient magnetic field records from ocean and lake sediments. Unlike other sources like lava flows or historical artifacts, which offer snapshots of the magnetic field at specific points in time, sediment records provide a continuous history that can span thousands to millions of years. However, interpreting the magnetic signal in sediments can be challenging due to various natural processes that occur during and after deposition or due to the way records are extracted. To correct the resulting inaccuracies, we present a method that accounts for various influencing factors and adjusts the sediment record. This correction process involves statistical techniques and independent magnetic information derived from archaeomagnetic data. We've tested *sedprep* with both synthetic data and real-world examples, showing that it can effectively reconstruct the main characteristics of the Earth's magnetic field from sediment records. The next steps involve applying *sedprep* to more datasets to validate its effectiveness and to help improve global models of the Earth's magnetic field.

1. Introduction

Sediment records are invaluable for reconstructing the geomagnetic field evolution over extensive timescales. Their comprehensive temporal and spatial coverage provide a richer dataset than the isolated snapshots offered by archaeomagnetic data and lava flows, making them essential in geomagnetic field modeling. However, the interpretation of sediment records is challenging due to potential distortions associated with the way sediments acquire magnetization and the procedures involved in core sampling and measurement. We will explore some of the most significant challenges and distortions in the following.

Magnetic declination describes the angle between the magnetic and geographical north. Declinations are commonly reported in relative values, primarily due to the absence of azimuthal core orientation during coring. Typically, the time series are oriented to zero mean. However, declination data is subject to additional uncertainties that are often not accounted for in many studies. For instance twisting of the core or multiple declination rotations between sub-sections or sub-cores, as seen in studies such for example, Verosub et al. (1986),

Visualization: L. Bohsung, M. Schanner
Writing – original draft: L. Bohsung
Writing – review & editing: L. Bohsung, M. Schanner, M. Korte, M. Holschneider

introduce complexities that cannot be simplified to a single declination rotation. Our approach addresses this by treating declination rotations for each sub-core or sub-section separately. The relationship between relative and absolute observations is established through the addition of a constant declination offset. Various methodologies have been employed for this transformation, including the utilization of absolute measurements derived from archaeomagnetic artifacts or volcanic rocks (e.g., Verosub et al., 1986) or the prediction from global or regional geomagnetic field models based on absolute measurements (e.g., Bohsung et al., 2024; Korte & Constable, 2011). Nilsson et al. (2014) applied a two-step correction process, adjusting sedimentary declination records based on comparisons with a prior dipole field model or nearby archaeomagnetic data. In Panovska et al. (2015) the estimation of the declination offsets is performed during the inversion rather than using prior adjustment.

Magnetic inclination, in the context of geomagnetism, refers to the angle between the geomagnetic field lines and the horizontal plane at a specific location. It provides a measure of the tilt of the magnetic field vector with respect to the Earth's surface. Inclination is measured in degrees and varies across the globe, with the magnetic field lines being vertical at the magnetic poles and horizontal at the magnetic equator.

The interpretation of inclination in sediments is not without challenges. One notable phenomenon is inclination shallowing, a distortion that occurs during the deposition when, for instance, non-spherical particles settle flat on the sediment/water interface. Inclination shallowing causes systematic underestimation of the true geomagnetic field inclinations (e.g., R. King, 1955; Kodama, 2012). R. King (1955) conducted laboratory experiments and described the degree of inclination shallowing by the following formula

$$f = \frac{\tan(I_o)}{\tan(I_f)} \tag{1}$$

where I_o represents the observed inclination, I_f the actual geomagnetic field inclination and $f \in (0, 1)$ the shallowing factor. A shallowing factor of 1 means no inclination shallowing. The smaller the shallowing factor becomes the stronger the inclination shallowing effect is.

Two correction methods exist: the first examines magnetic fabrics in sedimentary rocks pioneered by Jackson et al. (1991), refined by Bilardello (2015). The second, the statistical elongation/inclination (E-I) approach by Tauxe Kent (2004), uses the TK03.GAD model predicting elongated distributions based on palaeomagnetic data. The first method requires a lot of laboratory work and many measurements. While easy to use, challenges with the elongation/inclination (E-I) approach include the need for a substantial dataset and potential unsuitability for slow sedimentary settings.

The intensity recording in sediment records is influenced by many factors such as the concentration and mineralogy of ferrimagnetic material, and the magnetic domain-state of these particles. For instance, a sediment layer with a high magnetite content can exhibit strong remanence even if it was deposited under a weak magnetic field. Conversely, sediments with low magnetite content, like deep-sea carbonates or biosiliceous ooze, might record a weak signal despite a strong ambient magnetic field (Brachfeld, 2007). This makes it necessary to normalize the measured signal leading to relative paleointensity (RPI) values instead of absolute values. Additionally, coring disturbances can impact the sedimentary fabric, which in turn can reduce the RPI. Disturbances during the coring process, such as deformation or mixing of sediment layers, may disrupt the alignment of magnetic grains, leading to an underestimation of the recorded palaeointensity. To ensure the reliability of palaeointensity in sediment records, J. W. King et al. (1983) and Tauxe (1993) identified key criteria, including uniform magnetic mineralogy and grain sizes, clear demagnetization patterns, no correlation with general magnetic properties, and agreement across different normalization methods.

Several calibration methodologies have been proposed. Some methods utilize mean and minimum virtual axial dipole moments (e.g., Channell et al., 2009; Valet et al., 2005). Another way is the calibration against absolute intensity measurements generally obtained from volcanic rocks or archaeological artifacts, which are less affected by non-field factors. A more general approach is to use predictions from existing global or regional models, while one should make sure to use models that are based on absolute measurements (e.g., Korte & Constable, 2006).

The traditional post-Depositional Detrital Remanent Magnetization (pDRM) model, grounded in extensive research (e.g., Hamano, 1980; Irving, 1957; Kent, 1973; Otofuji & Sasajima, 1981), indicates that while coarse-grained sediment particles are fixed shortly after deposition, finer particles remain mobile in water-filled voids,

gradually becoming locked as the sediment consolidates. However, this classical concept faces challenges from theories suggesting limited post-depositional movement due to sediment flocculation and the impact of bioturbation (Egli & Zhao, 2015; Katari et al., 2000). Despite these debates, the consensus is that pDRM leads to a delayed and smoothed magnetic signal in sediment layers. This effect is mathematically represented by a convolution (or weighted average) of the geomagnetic field and a lock-in function (Roberts et al., 2013; Suganuma et al., 2011). In a series of recent publication (Nilsson et al., 2018, 2022; Nilsson & Suttie, 2021), the authors focused on quantifying the effects of pDRM and improving the resolution of sedimentary records by utilizing a Bayesian modeling technique and a class of lock-in functions.

In this paper we present a further development of the Bayesian modeling technique introduced in Bohsung et al. (2023) to estimate all the aforementioned parameters simultaneously. The methodology leverages global archaeomagnetic and volcanic data as an independent reference for the parameter estimation of a single local sediment record. While declination offset, inclination shallowing and calibration of relative palaeointensity do only affect the individual field components (declination, inclination, and intensity), the distortion caused by pDRM affects all components. Therefore, the simultaneous estimation of all parameters is crucial. Following the estimation process, we apply the parameters to preprocess the sediment record, implementing straightforward adjustments for declination offset, inclination shallowing, and intensity calibration, while employing a more sophisticated Gaussian process deconvolution (Tobar et al., 2023) to correct for pDRM effects.

In Section 2 we present the sediment preprocessing Python package *sedprep*, introducing the implemented priors, the lock-in functions and parameter optimization methods. The mathematical details and necessary formulas for reproduction are presented in Section 3. Section 4 contains extensive synthetic tests as well as results from applying the method to two real world sediment records. The results are discussed in Section 5.

2. Sediment Preprocessing Method (Sedprep)

This section outlines our methodology for calibrating relative declinations and palaeointensity, and minimizing distortions caused by inclination shallowing and pDRM effects. It involves estimating the associated parameters, followed by their application in preprocessing of the sediment record. The processes associated to these parameters are described and discussed in the introduction. The method is implemented in a sediment preprocessing Python package called *sedprep* (Bohsung & Schanner, 2024a, 2024b). We start by determining the parameterization we use for the effects described in the introduction. Subsequently, we describe our method used to estimate these parameters, followed by an outline on how to apply the estimated parameters in a final sediment preprocessing step.

2.1. Parameterization

To convert relative declinations to absolute values, a constant value is subtracted, called declination offset. For records consisting of several sub-cores or sub-sections, multiple declination offset parameters may be necessary. The inclination shallowing factor, f, is given in Equation 1. The calibration of relative palaeointensity involves a multiplicative factor assumed to be constant across the whole sediment record.

The distortion due to pDRM is characterized by parameters defining the lock-in function. In Bohsung et al. (2023) the following new class of parameterized lock-in functions was proposed

$$F_{b_1,b_2,b_3,b_4}(z) = \frac{2}{-b_1 - b_2 + b_3 + b_4} \begin{cases} 0 & z \le b_1 \\ \dfrac{z - b_1}{b_2 - b_1} & b_1 < z \le b_2 \\ 1 & b_2 < z \le b_3 \\ \dfrac{b_4 - z}{b_4 - b_3} & b_3 < z \le b_4 \\ 0 & b_4 \le z \end{cases} \tag{2}$$

These lock-in functions model a wide range of possible lock-in behaviors including the offset and smoothing effect. The shape of the lock-in function is determined by the four non-negative and sequentially ordered

parameters $b_1, \ldots, b_4$. A few examples, illustrating their diversity and flexibility, can be found in Figures 4 and 5 of Bohsung et al. (2023). However, this flexibility comes at the cost of increased computational time and memory usage due to the need to optimize four parameters. To address this, we explored reducing the number of parameters from four to two by considering symmetric lock-in functions shaped like triangles or squares. Ultimately, we opted for symmetric trapezoid lock-in functions with fixed shape, defined by two parameters, a_1 and a_2, striking a balance between flexibility and computational efficiency. Each of the trapezoid lock-in functions is uniquely determined by two parameters a_1, determining the left vertex and a_2, determining the center of the trapezoid. The second vertex of the trapezoid (b_2 in the four-parameter case) is chosen directly in the middle between a_1 and a_2. Therefore, the half lock-in depth is indicated by the parameter a_2 and can directly be interpreted as the shift associated to the pDRM process. The reparameterization of the four parameters is given by

$$b_1 = a_1, \quad b_2 = \frac{a_1 + a_2}{2}, \quad b_3 = \frac{3a_2 - a_1}{2}, \quad b_4 = 2a_2 - a_1$$

Hence, the class of trapezoid lock-in functions is given by

$$F_{a_1,a_2}(z) = \frac{2}{3(a_2 - a_1)} \begin{cases} 0 & z \le a_1 \\ 2\dfrac{z - a_1}{a_2 - a_1} & a_1 < z \le \dfrac{a_1 + a_2}{2} \\ 1 & \dfrac{a_1 + a_2}{2} < z \le \dfrac{3a_2 - a_1}{2} \\ 2\dfrac{2a_2 - a_1 - z}{a_2 - a_1} & \dfrac{3a_2 - a_1}{2} < z \le 2a_2 - a_1 \\ 0 & 2a_2 - a_1 \le z \end{cases} \tag{3}$$

Both, the four-parameter and the simplified two-parameter trapezoid lock-in function classes, are implemented in the Python package *sedprep*. Additionally, we provide the possibility of estimating individual lock-in functions for the directional components (declination and inclination) and RPI. This is crucial as the quality of RPI measurements often varies compared to directional components and their uncertainties are often unknown (Roberts et al., 2013).

In summary, the estimation process includes declination offset parameters for converting relative to absolute declinations, one parameter for inclination shallowing, one for palaeointensity calibration and a variable number (eight, four or two) for the distortions associated to pDRM effects.

2.2. Parameter Estimation

As described in the introduction there are several ways of estimating parameters like the calibration factor or the shallowing factor. In most cases these methods use independent magnetic information from archaeomagnetic data or lava flows. Other methods utilize virtual axial dipole models or (local) models derived from independent magnetic data. Our method can be seen as a combination of these ways. We get the independent magnetic information from a global dataset of archaeomagnetic data and lava flows. This information together with prior assumptions on the geomagnetic field is used in a Bayesian modeling technique based on Gaussian processes to estimate the parameters described above. Internally, a global process based on the archaeomagnetic data and the prior assumptions is used as a reference for the sediment record. In contrast to many existing approaches our method respects prior uncertainties, measurement uncertainties and temporal uncertainties for archaeomagnetic data and the sediment record. Another big advantage of our method is the simultaneous estimation of all important parameters. This is similar to what Nilsson and Suttie (2021); Nilsson et al. (2022) did in the scope of geomagnetic field modeling. A detailed discussion of similarities and differences can be found in Section 5.

Figure 1 illustrates schematically and in a very simplified way, how the method works. The method is initialized by (a) a global dataset of independent magnetic information from archaeomagnetic data and lava flows; (b) prior assumptions on the geomagnetic field; and (c) prepared data from a specific sediment record. The data preparation includes transformation of maximum angular deviation (MAD) or α_{95} values into declination and inclination uncertainties, outlier removal, and the generation of an age-depth model. Besides the data and prior assumptions,

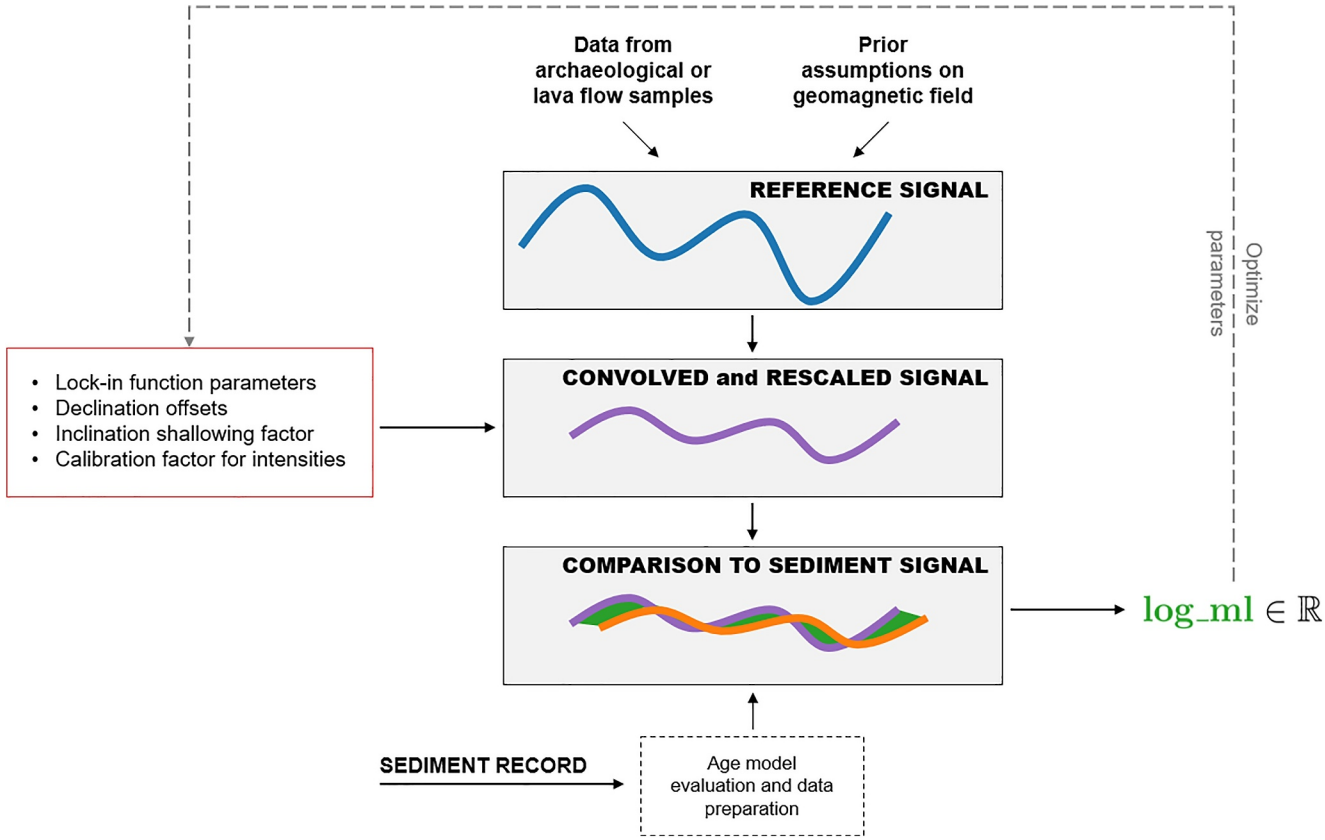

Figure 1. The figure shows a very simplified visualization of the proposed method. Internally, the method applies several parameters (red box) to the combined signal of independent magnetic information and prior assumptions (blue). The modified signal (purple) is then compared to the signal for a single sediment record (orange). The resulting *log_ml* value (green) can be interpreted as a measurement of agreement for a given set of parameters. By optimizing the *log_ml* value we can find the best set of input parameters.

a set of input parameters is fed into the method (red box). These input parameters are applied to the signal derived from the independent paleomagnetic data and the prior assumptions (see Section 2.1 for details about the parameters and Section 3 for details about the application of the parameters to the signal). The resulting signal (purple $\approx$ blue $\circ$ red) is then compared to the signal derived from the sediment record (orange). The method returns a single value which can be seen as a measurement of agreement between the modified reference signal and the signal derived from the sediment record. Our goal is to optimize this value by varying the input parameters. Details about the optimization process are given below.

The parameter estimation is done using a maximum likelihood estimation (type-II MLE (Rasmussen, 2004),). For computational reasons we replace the closed form Gaussian process regression by a Kalman filter (Kalman, 1960). The closed form marginal likelihood is approximated by a sum over the marginal likelihood values calculated for the individual Kalman filter steps (see Theorem 12.1 in Särkkä (2013)). The resulting expression provides a measure of how well a set of parameters describes the distortions in a single sediment record. For more details, especially about the modifications made to the standard Kalman Filter see Schanner et al. (2022) and Bohsung et al. (2023). To include the estimation of declination offsets, inclination shallowing and calibration factor for relative palaeointensity, an updated data model is needed. The details are described in Section 3.

To optimize the log-marginal likelihood two optimization approaches are implemented. The first employs dlib's LIPO-TR function optimization algorithm (D. E. King, 2009; Malherbe & Vayatis, 2017), which is adept at finding global optima without requiring an initial guess. The second approach utilizes a wrapper for scipy's optimization algorithms (Virtanen et al., 2020), which necessitate an initial guess. For declination offset and inclination shallowing factor an initial guess can be calculated based on an axial dipole assumption. For the

calibration factor for intensities we also use an axial dipole assumption but with a fixed intensity value. Here we use a value of $-32.8\mu T$ estimated from globally distributed archaeomagnetic covering the Holocene. Other values are possible but since we are working on the Holocene time period we decided to use this value. However, for the lock-in function parameters determining an initial guess is less straightforward. Therefore, we recommend using dlib with fixed declination offsets, inclination shallowing factor and calibration factor for intensities to determine a global optimum for the lock-in function parameters. Subsequently, the dlib result for the lock-in function parameters together with the axial dipole estimations for the remaining parameters can be used as initial guesses to optimize all parameters simultaneously utilizing one of scipy's optimization algorithms. To ensure convergence one should always check the gradients at the estimated optimum.

Most optimization algorithms require bounds for the individual parameters. The default implemented bounds are ± 180 for the declination offsets. The inclination shallowing factor is constrained between 0 and 1 and the bounds for the calibration factor is set to ± 3 standard deviations of the initial guess. For the lock-in function parameters the lower bounds are set to 0. The upper bounds require setting a maximal lock-in depth. We recommend starting with a minimum value of at least 50 cm. If the estimated lock-in function approaches this limit, we advise increasing the upper bound to ensure accurate modeling.

2.3. Correction of Data Distortion

Once all parameters are estimated, they are applied to the raw sediment data to calibrate and correct for the various distortions. For declination adjustments, we subtract the estimated declination offsets from each corresponding sub-section. The correction for inclination involves recalculating the raw inclination values, I_o, utilizing the formula $\arctan\left(\frac{\tan(I_o)}{f}\right)$, where f denotes the estimated shallowing factor. To calibrate relative palaeointensities we multiply it with the estimated calibration factor. In other words, correction of these distortion types are achieved by applying the respective inverse functionals. The pDRM effect leads to a convolved signal, where the estimated lock-in function represents the filter or impulse response and the source is represented by the magnetic field in form of a Gaussian process. To deconvolve the signal, we employ a Gaussian process deconvolution (Tobar et al., 2023) as an approximation for the inverse of the convolution functional.

3. Data Model

In this section we present the data model for the sediment data, which describes the relation between the measured signal in the sediment records and the geomagnetic field variations. We will use a modified and further developed data model based on the version presented in Bohsung et al. (2023). This section is structured as follows. We will start by summarizing the definitions of Bohsung et al. (2023). Subsequently, we will define additional functionals that are associated to declination offset, inclination shallowing and calibration of intensity. Finally, we will derive and present the new data model. We use the following notation: $C(\mathbb{R}, \mathbb{R}^3)$ denotes the set of all continuous functions from $\mathbb{R} \to \mathbb{R}^3$ and $\mathbf{G} \in C(\mathbb{R}, \mathbb{R}^3)$ denotes such a function. In addition, we define $C(\mathbb{R}, \mathbb{R})$ as the set of all continuous functions from $\mathbb{R} \to \mathbb{R}$ and by $H \in C(\mathbb{R}, \mathbb{R})$ we denote such a function.

The first functional defined in Bohsung et al. (2023) was the lock-in functional, denoted by $\mathfrak{F}_z$. However, we will change the notation here to $\mathfrak{L}_z$. The functional is defined as

$$\mathfrak{L}_z : C(\mathbb{R}, \mathbb{R}^3) \to \mathbb{R}^3 \qquad (z \mapsto \mathbf{G}(z)) \mapsto \int_0^\lambda \mathbf{G}\left(z - z'\right) F\left(z'\right) dz'$$

where $\lambda > 0$ is the lock-in depth and $F : \mathbb{R} \to \mathbb{R}$ is a lock-in function, that is, one out of the classes defined in Section 2.

The next functionals that we are going to use are the functionals that transform Cartesian field vector components (North (N), East (E), Down (Z)) into two angles, declination (D) and inclination (I), and intensity (F). The non-linear relationships between these components can be described by three observation functionals

$$\mathfrak{H}_z^D : \mathcal{C}(\mathbb{R}, \mathbb{R}^3) \to \mathbb{R} \qquad (z \mapsto \mathbf{G}(z)) \mapsto \arctan\left(\frac{\mathbf{G}_E(z)}{\mathbf{G}_N(z)}\right)$$

$$\mathfrak{H}_z^I : \mathcal{C}(\mathbb{R}, \mathbb{R}^3) \to \mathbb{R} \qquad (z \mapsto \mathrm{G}(z)) \mapsto \arctan\left(\frac{\mathbf{G}_Z(z)}{\sqrt{\mathbf{G}_N^2(z) + \mathbf{G}_E^2(z)}}\right)$$

$$\mathfrak{H}_z^F : \mathcal{C}(\mathbb{R}, \mathbb{R}^3) \to \mathbb{R} \qquad (z \mapsto \mathbf{G}(z)) \mapsto \sqrt{\mathbf{G}_E^2(z) + \mathbf{G}_N^2(z) + \mathbf{G}_Z^2(z)}$$

Note that one should use *arctan*2 for implementation since declination can take values from −180 to 180.

To incorporate declination offset, inclination shallowing and calibration of relative palaeointensities into our data model we define the following three functionals

$$\mathfrak{D}_z : \mathcal{C}(\mathbb{R}, \mathbb{R}) \to \mathbb{R} \qquad (z \mapsto H(z)) \mapsto H(z) + d$$

$$\mathfrak{I}_z : \mathcal{C}(\mathbb{R}, \mathbb{R}) \to \mathbb{R} \qquad (z \mapsto H(z)) \mapsto \arctan(f \tan(H(z)))$$

$$\mathfrak{F}_z : \mathcal{C}(\mathbb{R}, \mathbb{R}) \to \mathbb{R} \qquad (z \mapsto H(z)) \mapsto cH(z)$$

where $d \in (-180, 180)$ denotes the declination offset, $f \in (0, 1]$ denotes the shallowing factor and $c \in \mathbb{R}_{>0}$ is the calibration factor transforming relative palaeointensities into absolute values.

Applying $\mathfrak{D}_z$ on $\mathfrak{H}_z^D$, $\mathfrak{I}_z$ on $\mathfrak{H}_z^D$ and $\mathfrak{H}_z^I$ on $\mathfrak{H}_z^F$, respectively, results in the following modified observation functionals

$$\mathfrak{DH}_z = \mathfrak{D}_z\left[\mathfrak{H}_z^D(\mathbf{G})\right] = \arctan\left(\frac{\mathbf{G}_E(z)}{\mathbf{G}_N(z)}\right) + d$$

$$\mathfrak{IH}_z = \mathfrak{I}_z\left[\mathfrak{H}_z^I(\mathbf{G})\right] = \arctan\left(f\frac{\mathbf{G}_Z(z)}{\sqrt{\mathbf{G}_N^2(z) + \mathbf{G}_E^2(z)}}\right)$$

$$\mathfrak{FH}_z = \mathfrak{F}_z\left[\mathfrak{H}_z^F(\mathbf{G})\right] = c\sqrt{\mathbf{G}_E^2(z) + \mathbf{G}_N^2(z) + \mathbf{G}_Z^2(z)}$$

Analogously to Hellio et al. (2014) and Schanner et al. (2022) these functionals are linearized using a first order Taylor expansion. The data model follows directly from applying all of these functionals to the Gaussian process corresponding to the geomagnetic field.

4. Results

4.1. Synthetic Tests

To evaluate our method, we conducted synthetic tests using data based on an artificial reference geomagnetic field process. Three synthetic datasets were generated from this reference process. The first dataset represents the archaeomagnetic data with temporal and spatial distributions visualized in Figure 2 (upper panel and blue dots). These distributions as well as their temporal and measurement uncertainties coincide with the dataset of real archaeomagnetic data used in Section 4.2. Additionally, two synthetic sediment datasets were created. One represents a sediment record from Sweden (60°9′3.6″ N, 13°3′18″ E), and the other from Rapa Iti (27°36′57.6″ S, 144°16′58.8″ W) The decision for these two locations is based on the fact that the area around Sweden is well covered with archaeomagnetic data while the data coverage around Rapa Iti is sparse. Both datasets follow the same temporal distribution shown in the lower left panel of Figure 2. Their age-depth models are derived from the age-depth model of the sediment record FUR (L. M. Zillén et al., 2002; L. Zillén et al., 2003) which can be found in (Bohsung et al., 2023). Also, the uncertainties used to sample the synthetic sediment data are derived from this record, to reflect realistic scenarios.

To evaluate our method's ability to estimate multiple declination offsets, we divided the two synthetic sediment datasets into sub-sections *A1* and *A2*. These reflect real-world scenarios where sediment records may consist of

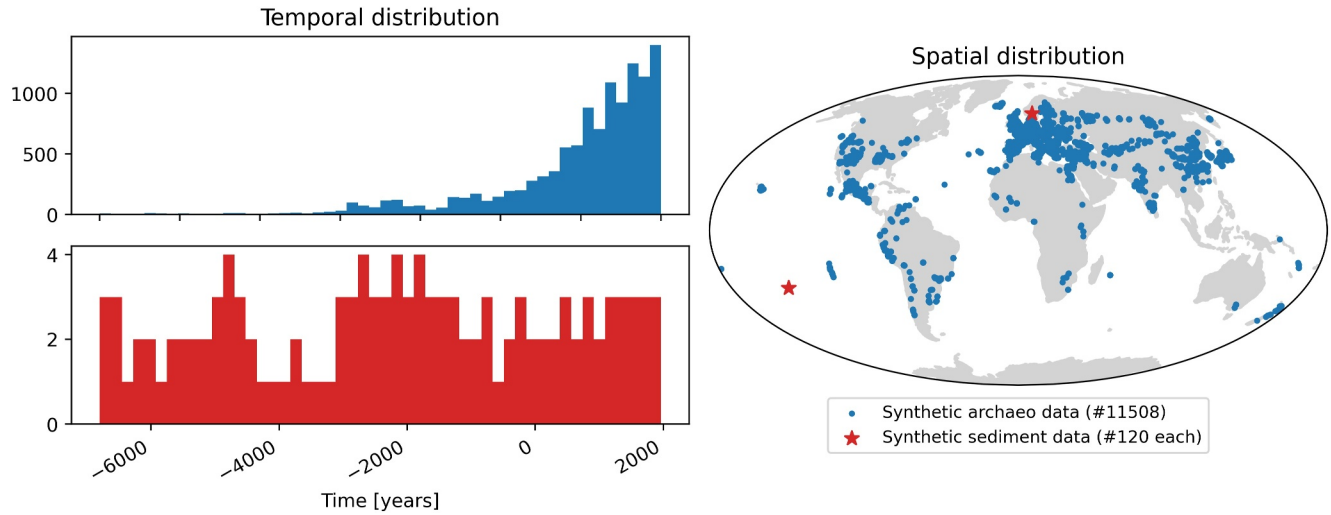

Figure 2. Spatial and temporal distribution of synthetic data. The upper panel on the left side shows the temporal distribution of the synthetic archaeomagnetic data while the temporal distribution for the synthetic sediment data is shown in the lower panel. Spatial distributions for synthetic archaeomagnetic data (blue dots) and the two synthetic sediment locations (red stars) are shown on the right side.

several sub-cores or sub-sections. We then applied specific distortions: offsets of 30° for *A1* and -10° for *A2*, a strong inclination shallowing factor of 0.6, and transformed intensities into relative values using a factor of $\frac{1}{90}$. To simulate the distortion associated to pDRM effects, three different lock-in functions with four-parameters were applied. The lock-in functions are shaped like a triangle, a square and a decreasing ramp.

In summary, the synthetic tests simulate six scenarios with varying lock-in functions and locations. Additional tests with different declination offsets, inclination shallowing factors, and calibration factors were conducted but are omitted here due to lack of additional insights.

For each of the six synthetic test cases we conducted two parameter estimations, applying both the four-parameter and the two-parameter lock-in function class. The lock-in function used to generate the data is in some cases not completely reproducible by lock-in functions from the two-parameter class. Additionally, we estimated the parameters for directional components and intensities separately. This is motivated by real-world scenarios, where the quality of directional measurements generally exceeds that of RPI data. Our method's ability of separate parameter estimation not only aligns with the typical quality disparity in sedimentary data but also reduces the parameter space dimension for the optimization process.

The results for one of the synthetic tests (located in Sweden with triangle-shaped lock-in function used for distortion) are visualized in Figure 3. The remaining results can be found in the Supplementary Information. The figure shows the results for both estimation procedures, the one using the four-parameter lock-in function (denoted by 4p and colored in blue) and the one using the two-parameter lock-in function (denoted by 2p and colored in purple). The three main panels display declination, inclination and intensity or RPI of the reference process (green line), the distorted synthetic sediment data with uncertainties (red and orange points), and the preprocessed sediment data (blue for the four-parameter case and purple for the two-parameter case). The boxes on the left side show the real parameters used for distortion and the estimated parameters for both cases. On the right, the lock-in function used for distortion (green) as well as the estimated lock-in functions (blue for the four-parameter and purple for the two-parameter case) are shown. As described above we used the same lock-in function to distort directional components and intensity but performed independent estimations to show the ability of the method of estimating parameters for these components independently. While the lock-in functions derived for each component did not match exactly, their similarities validate the effectiveness of the independent estimation approach.

The discrepancy between the corrected declinations and the reference process around 150 cm is attributed to the smoothing effect introduced during the deconvolution process. As described in Section 2.3, we apply a Gaussian process deconvolution to clean and correct the sediment data with respect to the pDRM effects. This approach

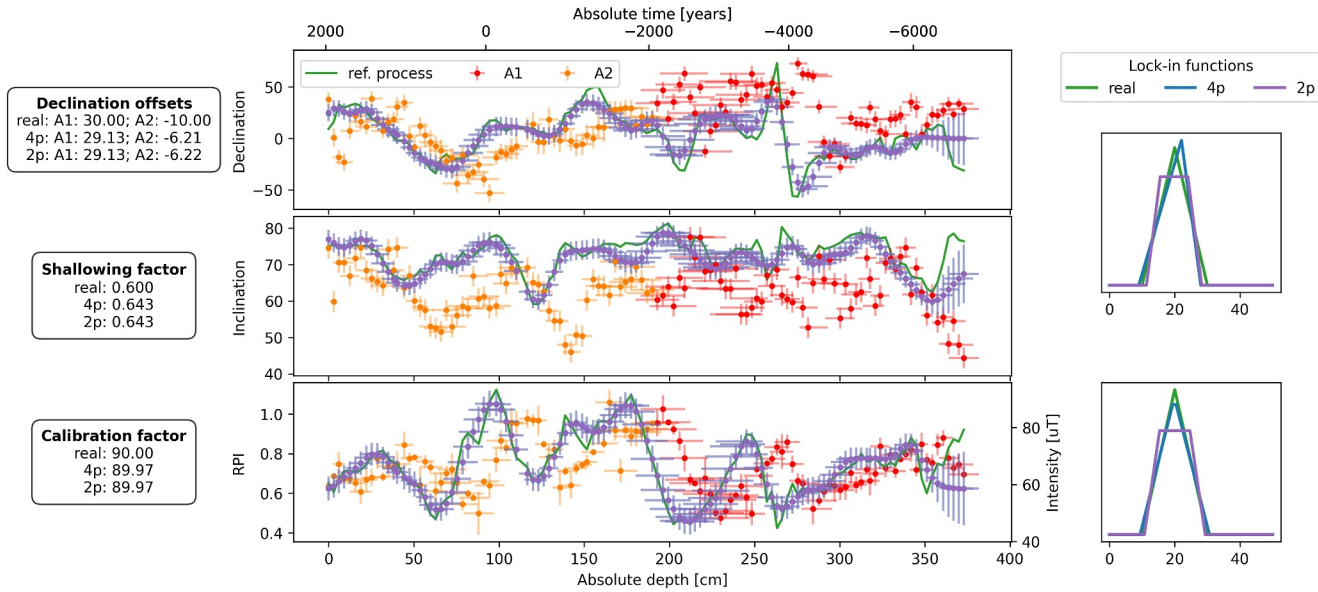

Figure 3. The figure shows the results for the synthetic test with location in Sweden and with the triangle-shaped lock-in function. The reference process is plotted as a green line, while the distorted sediment data points, shown with uncertainties (one standard deviation), are marked in red (sub-section *A1*) and orange (sub-section *A2*). The corrected sediment data are indicated in blue for the four-parameter lock-in function estimation and in purple for the two-parameter estimation. In this specific example, the blue points are not visible since they are covered by the purple ones. The lock-in functions themselves are shown on the right: the real lock-in function used for distortion in green, and the estimated lock-in functions in blue (four-parameter case) and purple (two-parameter case). The inset boxes on the left side detail the actual parameters used for distortion alongside the corresponding estimations for both lock-in function scenarios.

inherently introduces some degree of smoothing due to the nature of the Gaussian process. This smoothing can cause the corrected signal to appear less sharp and slightly deviate from the true signal, particularly in regions where there are rapid changes or variations in the original data. However, this smoothing effect is known and is reflected in the increased uncertainties associated with the corrected data, ensuring that the deconvolved signal appropriately accounts for the potential loss of finer variations.

Analysis of the lock-in function parameter estimation in Bohsung et al. (2024) found that some parameters are better constrained than others. Aside from lower computational cost, this motivated the investigation of the alternative two parameter lock-in function. In order to assess this effect in the present study, we perform a brief uncertainty analysis. Based on the observed Fisher information and the Cramér-Rao lower bound, the variance of the estimated parameters can be gauged by the inverse of the Hessian matrix of the marginal likelihood (Dodge, 2003). Calculating the Hessian is computationally demanding. We therefore restrict ourselves to a brief analysis of only one test case, the triangle-shaped function in Sweden. The estimated uncertainties are presented in Table 1. Evidently, some individual lock-in function parameters in the four-parameter case show much higher uncertainties than the parameters of the lock-in function from the two-parameter class. An eigenvalue decomposition of the four parameter Hessian reveals, that combinations of the four parameters are better constrained than the individual values. This supports the idea of shifting to a more interpretable parameterization by the half lock-in depth, as provided by the two-parameter class.

Table 1
Uncertainty Estimations for Estimated Parameters in the Four-Parameter and Two-Parameter Case

b_1	b_2	b_3	b_4	o_{A1}	o_{A2}	f
3.273	8.040	2.241	9.352	2.359	1.705	0.017
	2.884	2.503		2.359	1.705	0.017
	a_1	a_2		o_{A1}	o_{A2}	f

b_*: lock-in function parameter for the four-parameter case

a_*: lock-in function parameter for the two-parameter case

o_*: declination offsets

f: shallowing factor

4.2. Application to Real Data

The focus of this paper is primarily the introduction and validation of the Python package *sedprep* and the underlying method. A comprehensive application to many more datasets will be done in a future study. Nevertheless, to substantiate the efficacy of the method beyond synthetic tests, we conducted a preliminary application on two real datasets previously used in Bohsung et al. (2024): BIR (Frank et al., 2003; Schwab et al., 2004) and FUR_P2 (L. M. Zillén et al., 2002; L. Zillén et al., 2003).

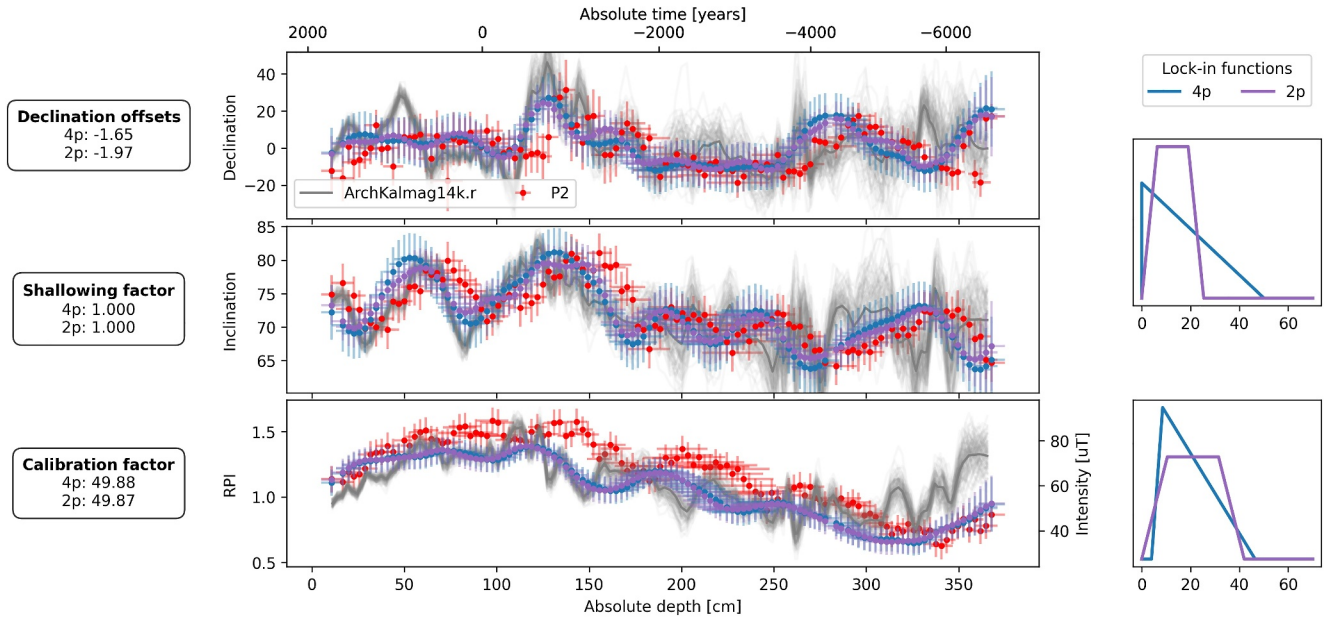

Figure 4. The figure shows the results for the FUR_P2 record. The sediment data points, shown with uncertainties, are marked in red. The corrected sediment data are indicated in blue for the four-parameter lock-in function estimation and in purple for the two-parameter estimation. The gray lines are mean and one hundred samples from the ArchKalmag14k.r model. The two estimated lock-in functions are shown on the right: in blue for the four-parameter case and purple for the two-parameter case. The boxes on the left side detail the estimated parameters for both lock-in function scenarios.

These datasets were selected for their diversity in representing a broad spectrum of effects appearing in real sediment data that our method is able to handle. The raw data for both records are accessible via the GEOMAGIA database (Brown et al., 2015). Both records have a solid number of radiocarbon dates and therefore reliable age-depth models that are independent of magnetic measurements. Here we use the same age-depth models and data preparation procedure as in Bohsung et al. (2024). From FUR_P2 we investigate all three components, that is, declination, inclination, and intensity, while we focus on directional components of BIR. The reason is that the sediments are not suitable for estimating RPI (see Section 4.4 of Frank et al. (2003)). In the absence of specific measurement uncertainties for the RPI in FUR_P2, we use a uniform uncertainty value of 0.1. Consistent with the approach taken for synthetic data, we estimated the parameters for directional components (declination and inclination) separately from those for intensity. This decision is justified by the typically lower precision of intensity measurements and the absence of corresponding uncertainties.

For the parameter estimation we used the axial dipole assumption to determine initial values for declination offsets, shallowing factor and an axial dipole assumption with fixed intensity of -32.8μT for the calibration factor for intensities (see Section 2.2). Then we fixed these values and used dlib to find a global optimum for the lock-in function parameters. Subsequently, we optimized all parameters simultaneously utilizing scipy's implementation of the Nelder-Mead optimization algorithm with upper bounds of 100 cm for all lock-in function parameters and default bounds for the remaining parameters. All these functionalities are implemented in a user-friendly setting and can be executed in a single function call. Visit our website for a detailed tutorial on how to use *sedprep* (Bohsung & Schanner, 2024b).

The FUR_P2 record is a sub-core of the FUR record, taken from the Lake Furskogstjärnet, located in the southern boreal forest region in Värmland, west central Sweden. The record covers approximately the last 9,000 years and consists of a single section. The results of the parameter estimation for this record are presented in Figure 4 together with mean and one hundred samples of the ArchKalmag14k.r model (Schanner et al., 2022) at the same geographical location as the sediment record. Given that this model is exclusively derived from archaeomagnetic data, it provides a pertinent benchmark for comparison. It is crucial to note that the model does not influence our methodology but is utilized here solely for graphical comparative purposes.

Although there appears to be some disparity between the estimated lock-in functions, the preprocessed sediment data from both (represented by blue and purple points) agree closely and align well with the ArchKalmag14k.r

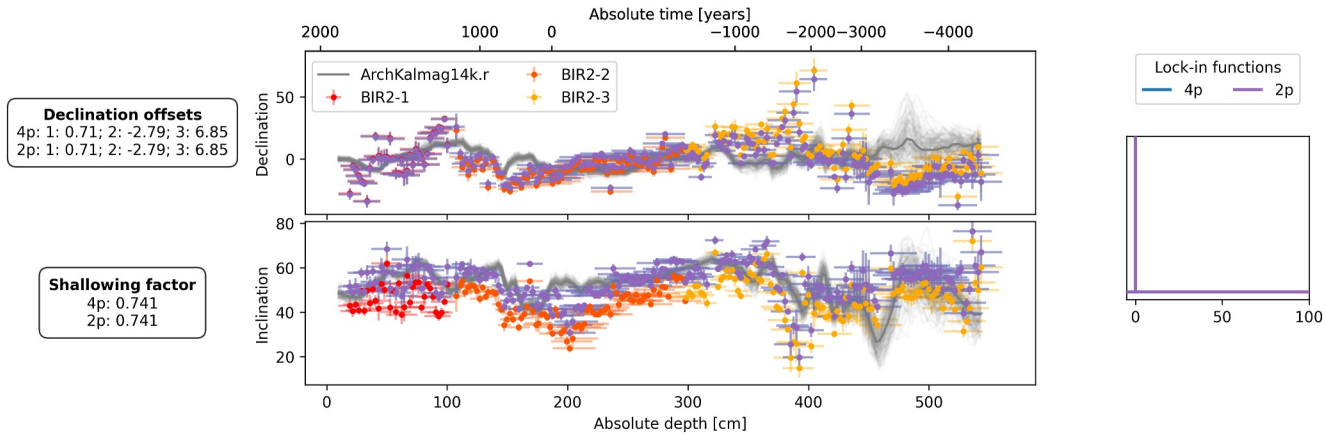

Figure 5. The figure shows the results for the BIR record.

model, particularly during periods of smaller model uncertainty. The observed discrepancies in the estimated lock-in functions are due to the fact that the two-parameter lock-in function cannot emulate a ramp effect like its four-parameter counterpart. Furthermore, the estimated shallowing factor implies the absence of inclination shallowing which agrees with the visual assessments of the data. Additionally, the calibrated intensity values exhibit satisfactory consistency with ArchKalmag14k.r, especially for more recent periods characterized by lower uncertainties.

The BIR record taken from the crater lake Birkat Ram in the northeastern Golan Heights covers approximately the last 6,000 years and consists of three sub-sections BIR2-1, BIR2-2 and BIR2-3. The results of the parameter estimation are presented in Figure 5. The three sub-sections are color-coded in red, orange and yellow.

The results suggest that the BIR record is unaffected by pDRM effects, as indicated by the estimated lock-in function from both the two-parameter and the four-parameter classes, which implies a deconvolution is not required for this dataset. A shallowing factor of 0.74 was estimated, indicating strong inclination shallowing. The declination offsets for the first two sub-sections were minor, while a more substantial shift was observed for the sub-section *BIR1-3*.

Some systematic differences remain between the corrected inclination signal and the ArchKalmag14k.r model predictions. In particular, the inclination discrepancies observed between 130 and 220 cm might reflect artifacts introduced by the age model. This depth interval is notable because bulk samples, rather than individual plant remains, were used for radiocarbon dating (as shown in Figure 9 in Bohsung et al. (2024)), potentially introducing age uncertainties that affect the alignment of the paleomagnetic data. Additionally, since inclination shallowing can be influenced by changes in remanence carrier properties, any variations in the size and/or shape of magnetic grains may affect inclination. Furthermore, depth-dependent changes in the sedimentary recording mechanism may contribute to these discrepancies. As sediment properties and remanence carriers vary with depth, the sedimentary layers within this interval might exhibit different recording efficiencies and inclination shallowing effects, complicating the application of a uniform lock-in function and shallowing factor across the record.

5. Discussion

In this study we present *sedprep*, a Python package based on a Bayesian modeling approach utilizing a global archaeomagnetic dataset for advanced sediment data preprocessing. Our validations via synthetic tests and real-world data applications underscore the method's robustness and versatility. The principal feature of *sedprep* lies in its capacity to simultaneously estimate various parameters associated with different distortions affecting sediment data and their magnetic signal. Besides the simultaneous estimation, the incorporation of uncertainties — both temporal and measurement-related — into our model is a critical advancement over previous methods. By utilizing a global archaeomagnetic dataset and prior assumptions on the geomagnetic field we are able to estimate parameters for sediment records at any global location without the need of a pretrained (local) model. Notwithstanding, the method faces limitations when extended beyond the Holocene due to the paucity of independent measurements in earlier periods, which can affect the robustness of estimations.

The synthetic tests as well as the application to real-world data reveal that our method adapts well across different scenarios, indicating its flexibility and utility. The synthetic tests yield a promising agreement with the reference process, successfully reconstructing main signal features even when the distorted data appeared deficient. Fast varying features of the reference process are sometimes lost especially in cases where the lock-in function has a large maximal lock-in depth. For real-world datasets, where a reference process is absent, comparisons with the ArchKalmag14k.r model suggest a markedly improved agreement after applying the estimated parameters.

5.1. Lock-in Function Classes

We have expanded the toolbox for modeling pDRM effects by introducing a second class of lock-in functions with only two parameters, in addition to the previously established four-parameter class (Bohsung et al., 2023). This reduction of parameter complexity comes with a decrease in flexibility, as evidenced by the ramp-shaped synthetic tests and the FUR_P2 record. However, the reconstruction of the main signal features are not significantly affected by the discrepancies between the two-parameter or four-parameter lock-in functions, justifying the use of both lock-in function classes. The ability (but not necessity) to individually estimate parameters for directional components and RPI is crucial, considering the general discrepancy in quality between these data types and the often unspecified uncertainties associated with RPI (Roberts et al., 2013).

The brief analysis of the uncertainty estimations of the estimated parameters indicates that lock-in function parameters in the two-parameter case are generally more accurately determined compared to the four-parameter case. This explains the high variance in estimated lock-in functions visible in Figures 4 and 5 in (Bohsung et al., 2023). Although the four-parameter class of lock-in functions offers higher flexibility, it is advised to focus on the overall shape rather than the precise values of each parameter. Conversely, the two-parameter case allows a more confident interpretation and reliability of the estimated parameters, particularly for a_2, which directly corresponds to the shift associated to the pDRM effect.

Our results on the lock-in function parameters support the findings in Nilsson et al. (2018); Nilsson and Suttie (2021); Nilsson et al. (2022). Their use of an MCMC approach allowed for direct sampling from the posterior distribution, providing a more detailed characterization of uncertainties associated with specific parameters of the lock-in function. Their findings, much like ours, indicate that while the exact shape of the lock-in function may not be as precisely determined, the half lock-in depth—and consequently the shift associated with the pDRM effect—tends to be well constrained.

5.2. It is Important to Notice That we use a Time-Averages

In our current approach, the lock-in function is assumed to be time-invariant across the entire sedimentary record, meaning it remains the same throughout the dataset. This might introduces potential limitations when dealing with variations in sedimentation material over time. Theoretically, it is possible to divide the sediment record into shorter sections and apply different lock-in functions to each. However, this presents challenges, including how to define these sections and manage transitions between them. Importantly, the lock-in functions of adjacent sections should not be treated as completely independent, as sedimentation processes are unlikely to change abruptly and completely. Therefore, determining the correlation between the lock-in functions of successive sections is necessary, making the approach less trivial. Further research is required to develop a method that appropriately accounts for these correlations while still allowing for the flexibility to model time-varying lock-in functions.

5.3. Estimated Declination Offset

In Bohsung et al. (2024) a new method of estimating declination offsets was introduced, leveraging the posterior distribution of ArchKalmag14k.r and a Type-II maximum likelihood estimation technique. Our method distinguishes itself in two significant ways. First, it operates independently of pretrained models, utilizing direct measurements from archaeomagnetic data and lava flow samples. This independence extends our method's applicability beyond the temporal constraints of pretrained models, though periods with more independent measurements enhance the likelihood of optimally estimated parameters. Second, our approach simultaneously estimates additional parameters, including lock-in function parameters which are associated to the pDRM effects. Since pDRM effects can lead to a horizontal shift it significantly influences the vertical declination offset estimations.

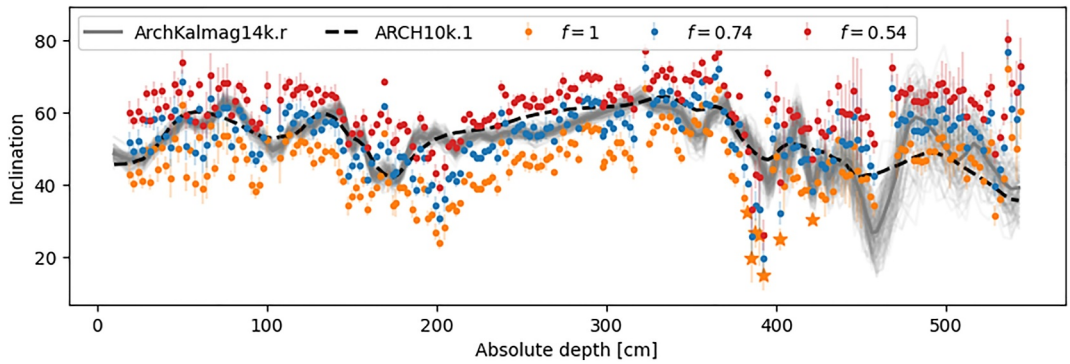

Figure 6. The figure shows three different inclinations of the BIR record, with the original inclination of the raw data in orange. Inclinations after applying shallowing factors of 0.74 and 0.54 are shown in blue and red, respectively. Additionally, predictions in form of mean and one hundred samples of ArchKalmag14k.r are visualized in gray and prediction of ARCH10k.1 in black.

In the future we will do a more detailed analysis of these two methods but for now we will just compare the estimated parameters for FUR_P2 and BIR from Bohsung et al. (2024) to the estimations made in this paper. The offset parameter estimated in this paper can be found in Figures 4 and 5. The estimated parameters using the method proposed in Bohsung et al. (2024) are given by, FUR_P2: −0.38, BIR2-1: 1.53, BIR2-2: −2.17, BIR2-3: 9.64. The differences range from a bit more than half a degree to almost three degrees. Just based on these two examples one can say that both methods deliver similar declination offsets. For a more comprehensive evaluation much more examples would be necessary.

5.4. Estimated Inclination Shallowing

The inclination shallowing factor estimated for the BIR records of 0.74 implies inclination shallowing. Compared to a shallowing factor of 0.54 estimated using the E/I-analysis tool Palaeomagnetism.org 2.4.0 (Jollyfant & Pastor-Galán, 2022; M. R. Koymans et al., 2016; M. Koymans et al., 2020), our method implies a more modest correction for inclination shallowing. In Figure 6, we compare these estimations against the uncorrected raw data and the predictions from two models, namely ArchKalmag14k.r (Schanner et al., 2022) and ARCH10k.1 (Constable et al., 2016). The uncorrected raw data, displayed in orange, reflects an obviously too shallow inclination. When adjusted with the E/I-derived shallowing factor of 0.54, the inclination does not consistently align with either of the models across most time intervals. In contrast, applying the factor derived from our method yields a closer match to both models, particularly during recent periods characterized by smaller uncertainties. Note that uncertainties are only available for ArchKalmag14k.r.

The discrepancy in shallowing factors between the two methods may stem from the E/I-method's neglection of uncertainties in its analysis. Consequently, deviations in inclination, such as the decrease observed at approximately 390 cm depth, disproportionately influences the shallowing factor estimation. This results in an underestimation, as the method does not sufficiently weigh the relative high uncertainties of these data points. By taking the uncertainties into account our method leads to a more representative and balanced estimation of the shallowing factor. This hypothesis was reinforced when we removing seven data points in this region. The excluded points are marked by orange stars in Figure 6. The recalculated shallowing factor using the E/I-method on this revised dataset was 0.73, aligning much more closely with our estimation.

5.5. Correction of Data Distortion

As described in Section 2, we use a Gaussian process deconvolution to apply the estimated lock-in functions. This technique results in a smoother signal which is visible in both the synthetic test and the FUR_P2 sediment record. Note, that lock-in functions with broader maximal lock-in depths imply stronger smoothing. Deconvolving a stronger smoothed signal results in greater posterior uncertainties. This is important as stronger smoothed records may not capture finer variations, thereby necessitating increased uncertainties to account for potential signal loss.

5.6. Advantages and Limitations in Comparison to Recent Approaches

Our Bayesian modeling technique shares several similarities with recent methods developed for analyzing post-depositional remanent magnetization (pDRM) in sediment records, particularly those presented in the Nilsson et al. (2018); Nilsson and Suttie (2021); Nilsson et al. (2022). Both approaches use archeomagnetic data as a reference and parameterize pDRM effects as a convolution of the geomagnetic field with a class of parameterized lock-in functions. Additionally, both methodologies allow for the simultaneous estimation of all relevant parameters. These shared characteristics indicate a common goal of improving the resolution and accuracy of sedimentary paleomagnetic records.

However, there are important distinctions between the two approaches that highlight the specific advantages and limitations of our method. One key difference is the scope of application. While Nilsson et al. focus on modeling multiple globally distributed sediment records simultaneously to produce a global geomagnetic field model, our approach concentrates on processing a single sediment record at a time. Additionally, in contrast to the approach presented by Nilsson et al. our approach accounts for Relative Palaeointensity (RPI). While their method co-estimates age-depth models alongside pDRM parameters, we rely on pre-computed age-depth models, which simplifies the process but may limit flexibility in certain contexts where the age model is less reliable. In Nilsson et al., the stratigraphy is directly incorporated by modeling the age-depth relationship, ensuring precise alignment with sedimentary layers. In our Kalman Filter approach, this is not directly possible. Instead, we divide the time series into 50 year chunks. Within each chunk, stratigraphic variations are not explicitly modeled, but the stratigraphy is respected between chunks.

A big differece is in the class of lock-in functions. Especially, our four-parameter class is offering a more flexible representation of smoothing and shift effects compared to their focus on linear, cubic, or exponetial lock-in functions, which can have a long tail. Moreover, while both approaches estimate a declination offset, our method uniquely accounts for sub-section specific declination offsets. Additionally, we incorporate an inclination shallowing factor according to Equation 1 while their approach uses a simple inclination correction offset similar to the declination offset. The use of a shallowing factor as presented in Equation 1 is especially interesting for records where inclination shallowing is a concern.

6. Conclusion

In this study we presented *sedprep*, a robust Python package for the preprocessing of sediment records. The application of *sedprep* to both synthetic tests and real-world datasets has demonstrated its effectiveness in addressing the multifaceted challenges associated with the interpretation of geomagnetic signals in sediment records. Looking forward, we aim to apply *sedprep* to a wide range of real-world data to further validate its utility and to perform a comparative analysis with sedimentological characteristics. Subsequently, a selection of the resulting preprocessed data will contribute to the development of an updated geomagnetic field model, integrating globally distributed sediment records as well as a set of global archaeomagnetic data.

Acknowledgments
This work was funded by the Deutsche Forschungsgemeinschaft (DFG, German Research Foundation), Grant 388291411. L. Bohsung and M. Schanner performed theoretical and conceptual work, with support of M. Korte and M. Holschneider. The manuscript was assembled by L. Bohsung with support from all co-authors. Software development and data processing was conducted by L. Bohsung and M. Schanner. The work and findings were supervised by M. Korte and M. Holschneider.This work utilized high-performance computing resources made possible by funding from the Ministry of Science, Research and Culture of the State of Brandenburg (MWFK) and are operated by the IT Services and Operations unit of the Helmholtz Centre Potsdam. Open Access funding enabled and organized by Projekt DEAL.

Data Availability Statement

The Python package *sedprep* is available as a git repository and can be found in the GitLab repository (Bohsung & Schanner, 2024a). All synthetic data sets used in this study are generated by us. The data sets together with python scripts used to generate the data can be found in the GitLab repository (Bohsung & Schanner, 2024a). The application to the two real-world data sets are available in form of a tutorial notebook on our website (Bohsung & Schanner, 2024b). The raw data for FUR_P2 and BIR are taken from GEOMAGIA (Brown et al., 2015).

References

Bilardello, D. (2015). Isolating the anisotropy of the characteristic remanence-carrying hematite grains: A first multispecimen approach. *Geophysical Journal International*, *202*(2), 695–712. https://doi.org/10.1093/gji/ggv171

Bohsung, L., & Schanner, M. (2024a). sedprep [Software]. Retrieved from https://git.gfz-potsdam.de/sec23/korte/sedprep

Bohsung, L., & Schanner, M. (2024b). sedprep: Palaeomagnetic sediment record preprocessing. [Website] https://sec23.git-pages.gfz-potsdam.de/korte/sedprep

Bohsung, L., Schanner, M., Korte, M., & Holschneider, M. (2023). Estimating post-depositional detrital remanent magnetization (pDRM) effects: A flexible lock-in function approach. *Journal of Geophysical Research: Solid Earth*, *128*(12), e2023JB027373. Retrieved from https://doi.org/10.1029/2023JB027373

Bohsung, L., Schanner, M., Korte, M., & Holschneider, M. (2024). Estimating post-depositional detrital remanent magnetization (pDRM) effects for several lacustrine and marine sediment records using a flexible lock-in function approach. *Journal of Geophysical Research: Solid Earth*, *129*(7), e2023JB027373. https://doi.org/10.1029/2024JB028864

Brachfeld, S. (2007). Paleointensity, relative, in sediments. In D. Gubbins & E. Herrero-Bervera (Eds.), *Encyclopedia of geomagnetism and paleomagnetism* (pp. 758–765). Dordrecht: Springer. Retrieved from https://doi.org/10.1007/978-1-4020-4423-6_253

Brown, M. C., Donadini, F., Nilsson, A., Panovska, S., Frank, U., Korhonen, K., et al. (2015). GEOMAGIA50. v3: 2. A new paleomagnetic database for lake and marine sediments. *Earth Planets and Space*, *67*, 1–19. https://doi.org/10.1186/s40623-015-0233-z

Channell, J., Xuan, C., & Hodell, D. (2009). Stacking paleointensity and oxygen isotope data for the last 1.5 Myr (PISO-1500). *Earth and Planetary Science Letters*, *283*(1–4), 14–23. https://doi.org/10.1016/j.epsl.2009.03.012

Constable, C., Korte, M., & Panovska, S. (2016). Persistent high paleosecular variation activity in southern hemisphere for at least 10 000 years. *Earth and Planetary Science Letters*, *453*, 78–86. Retrieved from https://doi.org/10.1016/j.epsl.2016.08.015

Dodge, Y. (2003). *The Oxford dictionary of statistical terms*. Oxford University Press.

Egli, R., & Zhao, X. (2015). Natural remanent magnetization acquisition in bioturbated sediment: General theory and implications for relative paleointensity reconstructions. *Geochemistry, Geophysics, Geosystems*, *16*(4), 995–1016. Retrieved from https://doi.org/10.1002/2014GC005672

Frank, U., Schwab, M. J., & Negendank, J. F. W. (2003). Results of rock magnetic investigations and relative paleointensity determinations on lacustrine sediments from Birkat Ram, Golan Heights (Israel). *Journal of Geophysical Research*, *108*(B8). Retrieved from https://doi.org/10.1029/2002JB002049

Hamano, Y. (1980). An experiment on the post-depositional remanent magnetization in artificial and natural sediments. *Earth and Planetary Science Letters*, *51*(1), 221–232. Retrieved from https://doi.org/10.1016/0012-821X(80)90270-8

Hellio, G., Gillet, N., Bouligand, C., & Jault, D. (2014). Stochastic modelling of regional archaeomagnetic series. *Geophysical Journal International*, *199*(2), 931–943. https://doi.org/10.1093/gji/ggu303

Irving, E. (1957). III. The origin of the palaeomagnetism of the Torridonian sandstones of north-west Scotland. *Philosophical Transactions of the Royal Society of London - Series A: Mathematical and Physical Sciences*, *250*(974), 100–110. https://doi.org/10.1098/rsta.1957.0014

Jackson, M. J., Banerjee, S. K., Marvin, J. A., Lu, R., & Gruber, W. (1991). Detrital remanence, inclination errors, and anhysteretic remanence anisotropy: Quantitative model and experimental results. *Geophysical Journal International*, *104*(1), 95–103. https://doi.org/10.1111/j.1365-246X.1991.tb02496.x

Jollyfant, & Pastor-Galán, D. (2022). *Jollyfant/PMAG2: v2.4.0*. Zenodo. https://doi.org/10.5281/zenodo.6380888

Kalman, R. E. (1960). A new approach to linear filtering and prediction problems. *Journal of Basic Engineering*, *82*(1), 35–45. https://doi.org/10.1115/1.3662552

Katari, K., Tauxe, L., & King, J. (2000). A reassessment of post-depositional remanent magnetism: Preliminary experiments with natural sediments. *Earth and Planetary Science Letters*, *183*(1), 147–160. Retrieved from https://doi.org/10.1016/S0012-821X(00)00255-7

Kent, D. V. (1973). Post-depositional remanent magnetisation in deep-sea sediment. *Nature*, *246*(5427), 32–34. https://doi.org/10.1038/246032a0

King, D. E. (2009). Dlib-ml: A machine learning toolkit. *Journal of Machine Learning Research*, *10*, 1755–1758.

King, J. W., Banerjee, S. K., & Marvin, J. (1983). A new rock-magnetic approach to selecting sediments for geomagnetic paleointensity studies: Application to paleointensity for the last 4000 years. *Journal of Geophysical Research*, *88*(B7), 5911–5921. https://doi.org/10.1029/JB088iB07p05911

King, R. (1955). The remanent magnetism of artificially deposited sediments. *Geophysical Supplements to the Monthly Notices of the Royal Astronomical Society*, *7*(3), 115–134. https://doi.org/10.1111/j.1365-246X.1955.tb06558.x

Kodama, K. P. (2012). *Paleomagnetism of sedimentary rocks: Process and interpretation*. John Wiley and Sons.

Korte, M., & Constable, C. (2006). On the use of calibrated relative paleointensity records to improve millennial-scale geomagnetic field models. *Geochemistry, Geophysics, Geosystems*, *7*(9). https://doi.org/10.1029/2006GC001368

Korte, M., & Constable, C. (2011). Improving geomagnetic field reconstructions for 0–3 ka. *Physics of the Earth and Planetary Interiors*, *188*(3–4), 247–259. https://doi.org/10.1016/j.pepi.2011.06.017

Koymans, M., van Hinsbergen, D., Pastor-Galán, D., Vaes, B., & Langereis, C. (2020). Towards FAIR paleomagnetic data management through Paleomagnetism. org 2.0. *Geochemistry, Geophysics, Geosystems*, *21*(2), e2019GC008838. https://doi.org/10.1029/2019GC008838

Koymans, M. R., Langereis, C. G., Pastor-Galán, D., & van Hinsbergen, D. J. (2016). *Paleomagnetism. org: An online multi-platform open source environment for paleomagnetic data analysis*. Elsevier. https://doi.org/10.1016/j.cageo.2016.05.007

Malherbe, C., & Vayatis, N. (2017). Global optimization of Lipschitz functions. In *International conference on machine learning* (pp. 2314–2323). https://doi.org/10.48550/arXiv.1703.02628

Nilsson, A., Holme, R., Korte, M., Suttie, N., & Hill, M. (2014). Reconstructing Holocene geomagnetic field variation: New methods, models and implications. *Geophysical Journal International*, *198*(1), 229–248. https://doi.org/10.1093/gji/ggu120

Nilsson, A., & Suttie, N. (2021). Probabilistic approach to geomagnetic field modelling of data with age uncertainties and post-depositional magnetisations. *Physics of the Earth and Planetary Interiors*, *317*, 106737. Retrieved from https://doi.org/10.1016/j.pepi.2021.106737

Nilsson, A., Suttie, N., & Hill, M. J. (2018). Short-term magnetic field variations from the post-depositional remanence of lake sediments. *Frontiers in Earth Science*, *6*, 39. https://doi.org/10.3389/feart.2018.00039

Nilsson, A., Suttie, N., Stoner, J. S., & Muscheler, R. (2022). Recurrent ancient geomagnetic field anomalies shed light on future evolution of the South Atlantic Anomaly. *Proceedings of the National Academy of Sciences*, *119*(24), e2200749119. Retrieved from https://doi.org/10.1073/pnas.2200749119

Otofuji, Y.-i., & Sasajima, S. (1981). A magnetization process of sediments: Laboratory experiments on post-depositional remanent magnetization. *Geophysical Journal International*, *66*(2), 241–259. Retrieved from https://doi.org/10.1111/j.1365-246X.1981.tb05955.x

Panovska, S., Korte, M., Finlay, C., & Constable, C. (2015). Limitations in paleomagnetic data and modelling techniques and their impact on Holocene geomagnetic field models. *Geophysical Journal International*, *202*(1), 402–418. https://doi.org/10.1093/gji/ggv137

Rasmussen, C. E. (2004). Gaussian processes in machine learning. In O. Bousquet, U. von Luxburg, & G. Rätsch (Eds.), *Advanced lectures on machine learning: Ml summer schools 2003, canberra, Australia, february 2 - 14, 2003, tübingen, Germany, august 4 - 16, 2003, revised lectures* (pp. 63–71). Springer Berlin Heidelberg. https://doi.org/10.1007/978-3-540-28650-9_4

Roberts, A. P., Tauxe, L., & Heslop, D. (2013). Magnetic paleointensity stratigraphy and high-resolution quaternary geochronology: Successes and future challenges. *Quaternary Science Reviews*, *61*, 1–16. Retrieved from https://doi.org/10.1016/j.quascirev.2012.10.036

Särkkä, S. (2013). *Bayesian filtering and smoothing*. Cambridge University Press. Retrieved from https://books.google.de/books?id=5VlsAAAAQBAJ

Schanner, M., Korte, M., & Holschneider, M. (2022). ArchKalmag14k: A kalman-filter based global geomagnetic model for the Holocene. *Journal of Geophysical Research: Solid Earth*, *127*(2), e2021JB023166. https://doi.org/10.1029/2021JB023166

Schwab, M. J., Neumann, F., Litt, T., Negendank, J. F., & Stein, M. (2004). Holocene palaeoecology of the golan Heights (near East): Investigation of lacustrine sediments from Birkat Ram crater lake. *Quaternary Science Reviews*, *23*(16–17), 1723–1731. https://doi.org/10.1016/j.quascirev.2004.05.001

Suganuma, Y., Okuno, J., Heslop, D., Roberts, A. P., Yamazaki, T., & Yokoyama, Y. (2011). Post-depositional remanent magnetization lock-in for marine sediments deduced from 10Be and paleomagnetic records through the Matuyama–Brunhes boundary. *Earth and Planetary Science Letters*, *311*(1), 39–52. Retrieved from https://doi.org/10.1016/j.epsl.2011.08.038

Tauxe, L. (1993). Sedimentary records of relative paleointensity of the geomagnetic field: Theory and practice. *Reviews of Geophysics*, *31*(3), 319–354. https://doi.org/10.1029/93RG01771

Tauxe, L., & Kent, D. V. (2004). A simplified statistical model for the geomagnetic field and the detection of shallow bias in paleomagnetic inclinations: Was the ancient magnetic field dipolar? *AGU Geophysical Monograph*, *145*, 101–115. https://doi.org/10.1029/145GM08

Tobar, F., Robert, A., & Silva, J. F. (2023). Gaussian process deconvolution. *Proceedings of the Royal Society A: Mathematical, Physical and Engineering Sciences*, *479*(2275). Retrieved from https://doi.org/10.1098/rspa.2022.0648

Valet, J.-P., Meynadier, L., & Guyodo, Y. (2005). Geomagnetic dipole strength and reversal rate over the past two million years. *Nature*, *435*(7043), 802–805. https://doi.org/10.1038/nature03674

Verosub, K. L., Mehringer, P. J., Jr., & Waterstraat, P. (1986). Holocene secular variation in western north America: Paleomagnetic record from fish lake, harney county, Oregon. *Journal of Geophysical Research*, *91*(B3), 3609–3623. https://doi.org/10.1029/JB091iB03p03609

Virtanen, P., Gommers, R., Oliphant, T. E., Haberland, M., Reddy, T., Cournapeau, D., & SciPy 1.0 Contributors. (2020). SciPy 1.0: Fundamental algorithms for scientific computing in Python. *Nature Methods*, *17*(3), 261–272. https://doi.org/10.1038/s41592-019-0686-2

Zillén, L., Snowball, I., Sandgren, P., & Stanton, T. (2003). Occurrence of varved lake sediment sequences in varmland, west central Sweden: Lake characteristics, varve chronology and AMS radiocarbon dating. *Boreas*, *32*(4), 612–626. https://doi.org/10.1080/03009480310004189

Zillén, L. M., Wastegård, S., & Snowball, I. F. (2002). Calendar year ages of three mid-Holocene tephra layers identified in varved lake sediments in west central Sweden. *Quaternary Science Reviews*, *21*(14–15), 1583–1591. https://doi.org/10.1016/S0277-3791(02)00036-7